Nanoscale

Accepted Manuscript

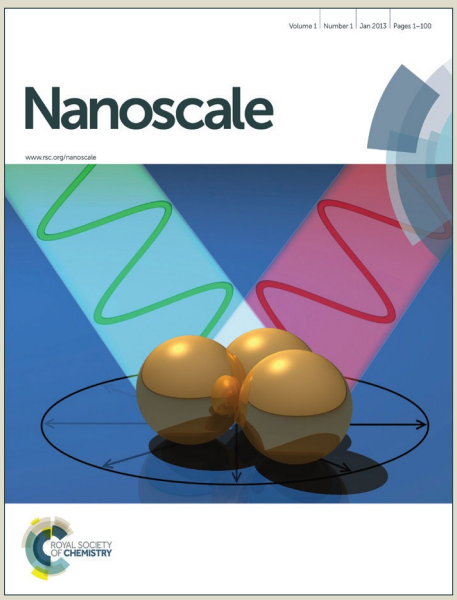

This is an *Accepted Manuscript*, which has been through the Royal Society of Chemistry peer review process and has been accepted for publication.

Accepted Manuscripts are published online shortly after acceptance, before technical editing, formatting and proof reading. Using this free service, authors can make their results available to the community, in citable form, before we publish the edited article. We will replace this *Accepted Manuscript* with the edited and formatted *Advance Article* as soon as it is available.

You can find more information about *Accepted Manuscripts* in the Information for Authors.

Please note that technical editing may introduce minor changes to the text and/or graphics, which may alter content. The journal's standard Terms & Conditions and the Ethical guidelines still apply. In no event shall the Royal Society of Chemistry be held responsible for any errors or omissions in this *Accepted Manuscript* or any consequences arising from the use of any information it contains.

ROYAL SOCIETY OF CHEMISTRY

www.rsc.org/nanoscale

Nanoscale

RSCPublishing

PAPER

Nanotubular structured Si-based multicomponent anodes for high-performance lithium-ion batteries with controllable pore size via coaxial electro-spinning

Cite this: DOI: 10.1039/x0xx00000x

Received 00th January 2014,
Accepted 00th January 2014

DOI: 10.1039/x0xx00000x

www.rsc.org/

Jaegeon Ryu, Sinho Choi, Taesoo Bok, and Soojin Park*

We demonstrate a simple but straightforward process for synthesis of nanotube-type Si-based multicomponents by combining a coaxial electrospinning technique and subsequent metallothermic reduction reaction. Si-based multicomponent anodes consisting of Si, alumina and titanium silicide show several advantages for high-performance lithium-ion batteries. Alumina and titanium silicide, which have high mechanical properties, act as an effective buffer layer for the large volume change of Si, resulting in outstanding volume suppression behavior (volume expansion of only 14%). Moreover, electrically conductive titanium silicide layers located at the inner and outer layers of a Si nanotube exhibit a high initial coulombic efficiency of 88.5% and extraordinary rate capability. Nanotubular structured Si-based multicomponents with mechanically and electrically improved components can be used as a promising alternative to conventional graphite anode materials. This synthetic route can be extended to other high capacity lithium-ion battery anode materials.

Introduction

Silicon (Si) has attracted much attention as one of the promising anode materials for next-generation lithium-ion batteries (LIBs) owing to its natural abundance and high theoretical specific capacity (3578 mA h g^{-1}, $Li_{3.75}Si$, at room temperature).[1] However, its cycling performance is unsatisfactory for practical use in LIBs because its huge volume expansion (>300%) upon repeated cycles results in severe pulverization, loss of electric contact, and dramatic capacity fading.[2, 3] Also, poor intrinsic properties of Si such as the low electronic conductivity (~10^{-3} S cm^{-1}) and slow lithium diffusion (diffusion coefficient 10^{-14} ~ 10^{-13} cm^2 s^{-1}) have impeded utilization of its full capacity and application to high power and energy density tools.[4-10]

To solve these critical problems, nanostructured Si, including nanoparticles,[11, 12] thin films,[13-16] nanowires,[17, 18] and hollow structures (*e.g.*, hollow spheres and nanotubes),[19-26] has been developed. Among these options, one-dimensional (1D) nanostructured Si-based materials have shown excellent electrochemical properties in LIBs for several reasons. First of all, they can accommodate the enormous volume expansion of Si and reduce the lithium ion diffusion pathway, due to their small axial dimension. Furthermore, they show improved electron transfer through the axis. This high lithium ion and electron transport kinetic can mediate the poor intrinsic conductivity of Si-based materials, leading to suitable applications in electronic devices requiring high power density.

Along with a growing need for 1D material, a great diversity of synthetic methods has been contrived. Top-down approach from chemical etching of Si wafers,[27, 28] chemical vapor deposition growth,[29-31] and electrospinning[32-34] are representative examples for synthesizing 1D Si-based materials. As repeatedly shown in the literature, polymeric and/or inorganic 1D nanofibers can be simply drawn out by means of the electrospinning process. Recently, Yoo et al. demonstrated synthesis of Si nanotubes by combining electrospun polyacrylonitrile nanofiber with silica coating and subsequent magnesiothermic reduction.[35] They used well-known method for preparing Si via magnesiothermic reduction of silicon dioxides. During the reduction, tremendous amount of heat was generated to cause structural disruption. That is why as-prepared Si nanotubes showed crushed and shrunken tubes. Unlike the magnesiothermic reduction, aluminothermic reduction using aluminium reductant, delivers less amount of heat. In view of the large-scale production, since batch size is directly proportionated to thermodynamically generated heat, aluminothermic reduction is a suitable process to increase the batch size. As another approach, Park et al. reported Si nanotube lithium-ion battery anodes with greatly enhanced electrochemical performances.[21] However, their process, combining an anodic aluminum oxide template with chemical reduction of organic Si precursor, was very expensive, low yield (<5%), and complicated multi-step process. Along with above technique, there are various methods for preparing a tubular structure, in particular SiO_2 nanotubes. Most of fabrications are based on template-assisted

Nanoscale Accepted Manuscript

or surfactant-aided preparation methods. Using different templates or surfactants such as metal oxides, metals, metal salts, carbon nanofibers, and organic surfactants, high purity and macro-/nano-dimensional SiO_2 nanotubes can be fabricated.[36-41] Furthermore, atomic layer deposition (ALD) can easily yield exceptionally conformal and uniform SiO_2 nanotubes by extent of atomic-level. Among them, one of the effective methods to prepare the tubular structure is coaxial electrospinning using dual nozzles with following advantages; (i) it is specialized to synthesize core/shell and hollow tubular organic and/or inorganic fibers in one-pot process,[42-48] (ii) it has the controllability on the wall and core size of nanotubes by simply tuning the flow rates and also we can easily add other metal oxide precursors to make hybrid materials in the preparation of electrospinning solution, and (iii) electrospinning technique can produce long-dimensional fibers with a high product yield for further processing. For these reasons, coaxial electrospinning method is one of the effective tools to synthesize tubular metal oxide and/or hybrid metal oxides. To the best of our knowledge, direct fabrication of Si-based nanotubes by the coaxial electrospinning method has not yet been reported.

In addition to nanostructuring of Si, numerous coating materials, including carbon materials,[49-54] metal,[55] metal oxide,[56] and metal silicide,[57, 58] have been introduced on the surface of Si-based materials. Most surface treatments have focused on either increasing mechanical property for Si anodes with a large volume change or enhancing electrical conductivity. Recently, Park et al. demonstrated that a metal silicide coating can significantly enhance both mechanical and electrical properties of micrometer-sized Si particles.[57] The metal silicide-coated Si anodes showed remarkably improved cycling stability and high rate capabilities. Those enhancements were attributed to increased electrical conductivity, good mechanical property, and a stable solid-electrolyte-interface formation.[57, 58] Furthermore, Memarzadeh et al. reported ALD method on Si nanotube prepared by sacrificial template. They also showed the effect of various coating materials (e.g., TiO_2, TiN, and Al_2O_3) on the electrochemical properties of Si nanotubes.[59] By ALD, coating level can be precisely controlled, thus it has been implemented to thin-film LIBs and also has great advantages for coating on the surface of irregularly nanostructured materials.[60] Among strategies mentioned above, a hybridized approach, combining structural and interfacial effects, is one of the effective methods to make high-performance Si battery anodes. However, nanotubular Si-based materials with both structural integrity and interfacial effect have not been described in other reports.

Herein, we demonstrate a one-pot synthetic route for nanotubular Si-based multicomponents utilizing two different well-known processes, coaxial electrospinning and subsequent aluminothermic reduction reaction. Coaxial electrospinning enables us to make a nanotubular structure of Si-containing materials, while the aluminothermic reaction can successfully convert silica to Si and form multicomponents including Si, alumina, and titanium silicide. The nanotubular Si-based multicomponent anodes show significantly improved electrochemical performances including increased initial coulombic efficiency (88.5%), cycling stability (~75% after 280 cycles), high rate capability (a specific capacity of 650 mAh g^{-1} at 5 C rate), and extremely suppressed volume expansion (~14% after 100 cycles) compared to bare Si nanotubes.

Experimental

Coaxial electrospinning process. For the core solution, heavy mineral oil was used (Aldrich). For the sheath solution, poly (vinyl pyrrolidone) (PVP, average Mw ~ 1300K, Aldrich) and tetraethyl orthosilicate (TEOS, Aldrich) were mixed together in ethanol solvent for enough time to form a transparent solution. In a typical process, the solutions were prepared by mixing 2.36 g of PVP, 3.0 g TEOS, 0.5 g Pluronic P123 (average Mn ~ 5,800, Aldrich), and 10 g absolute Ethanol, and then heated up to 80 ℃, simultaneously adding 0.1 g of 0.1 M HCl. It was injected to the outer syringe pump (NE - 1000, New Era Pump Systems) channel, and heavy mineral oil was added to the core syringe pump channel, connected to a metallic needle. These two types of solutions were fed at a certain constant rate. The optimized feeding rate of polymer solution was set at 0.9 mL/h. In addition, the oil rate was varied from 0.5 to 5 μL min^{-1}. Aluminum foil was placed 10 cm away from the needle to serve as a collector. All experiments were conducted at an accelerating voltage of 20 – 23 kV at room temperature in air. As-spun oil@polymer/SiO_2 fibers were peeled off from the collector, followed by natural drying at room temperature overnight for complete hydrolysis of TEOS. After drying, the collected fibers were immersed in n-hexane solution (Aldrich) for 24 hours to extract oil. Furthermore, pure SiO_2 nanotubes were obtained by calcination of polymer/SiO_2 nanotubes at 250 ^oC (5 ℃ min^{-1} rise) for 1 h (for stabilization) and 600 ^oC for 3 h (calcination of polymer and residual oil). In the TiO_2 coating system, 2 g of as-prepared SiO_2 nanotubes and 0.6 g hydroxypropylcelluose (average Mw ~ 100K, Aldrich) were well-dispersed in 100ml absolute ethanol for 30 min. Then, a certain amount of titanium butoxide (TB, Aldrich) was added to the above solution and it was further stirred for 2 h. With loading 1mL of DI water, TiO_2 was well coated on the in/out surface of the SiO_2 nanotubes. Finally, by heating these fibers up to 600 ^oC for 3 h, TiO_2 coated SiO_2 nanotubes can be obtained (Fig. S1 and Fig. S2b)

Aluminothermic reduction of SiO_2-based nanotubes. 1 g of TiO_2 coated SiO_2 nanotubes were mixed with 0.6 g of Al powder (3 – 5 μm) in ethanol so that the powders were uniformly mixed together. After completely drying out the solvent, the mixture was put on an alumina boat and placed in a tube furnace, heated up to 900 ^oC for 6 h under Ar atmosphere. Then, the product was leached out with concentrated H_3PO_4 and 0.5 M HF for eliminating undesirable materials such as an excess amount of Al_2O_3 and SiO_2. The fabricating condition for non-coated Silicon nanotubes is equivalent to the above experimental procedure except for the TiO_2 coating process. The carbon coating process was conducted by thermal deposition of toluene vapor at 900 ^oC for 8 min

Characterizations. Morphology of tubular Si nanotubes and different coating layers were characterized by scanning electron microscope (Verios 460, FEI) at an accelerating voltage of 10 kV, transmission electron microscopy (TEM, JEM-2100) at an acceleration voltage of 120kV, and high – resolution transmission electron microscopy (HR-TEM, JEM-2100F). TEM (JEM-2100)

Nanoscale Accepted Manuscript

 This journal is © The Royal Society of Chemistry 2014

was also used to investigate tube structures before and after cycling. A carbon coating layer on Si nanotube was characterized by Raman spectrometry (Alpha 300s, WITec GmbH) operating with a laser excitation wavelength of 532 nm and elemental analysis. X-ray diffraction (D8 ADVANCE, Bruker) was used to investigate tubular typed silicon nanotubes with titanium silicide coating layers.

Electrochemical test. The battery performance was measured by galvanostatic cycling (WonATech WBCS 3000 battery measurement system) of coin cells with the fabricated titanium silicide coated silicon nanotubes along with carbon coated and non-coated silicon nanotubes as the working electrode and lithium foil as the reference / counter electrode. The working electrodes were prepared using a conventional slurry method with a series of silicon nanotubes, super P, 1:1 mixture of poly (acrylic acid) (PAA, weigh average molecular weight ~100K, Aldrich), and sodium carboxymethyl cellulose (CMC, 4 wt% in H_2O, Aldrich) as a binder with a mass ratio of 7:1.5:1.5. The mass loading of active materials, except binder and conducting agent, was ~ 1.59 mg cm^{-2} and ~ 2.45 mAh cm^{-2}. The potential windows for all cycled cells were between 0.01 and 1.2 V versus Li/Li^+. The electrolyte comprised 1.3M LiPF6 in 3:7 v/v ethylene carbonate / diethyl carbonate with 10 wt% fluorinated ethylene carbonate additives to improve the cycling stability. Polyethylene film (Celgard 2400) was used as a separator. These were all carefully assembled in an Ar-filled glove box. After cycling, each cell was opened in the glove box and washed with dimethyl carbonate to remove residual electrolyte and any other impurities. Then it was dried at room temperature. EIS measurement was carried out between 10000 – 0.1 Hz with an amplitude of 10 mV at a fully-delithiated state (~ 1.2V).

Results and discussion

Synthesis of nanotubular Si-based multicomponents

The typical set up for coaxial electrospinning is illustrated in Fig. 1a. Two types of liquids were fed into a metallic dual nozzle with two channels connected to a spinneret. For the inner core part, heavy mineral oil was fed at a rate ranging from 0.5 to 5 μL min^{-1}. For the outer sheath part, we prepared a polymer solution containing poly(vinyl pyrrolidone) (PVP) and tetraethoxysilane as a silica source in absolute ethanol. Under a moderate electric field of 20-23 kV, core@shell (oil@polymer/SiO_2) nanofibers were drawn out. After oil extraction by n-hexane and subsequent calcination, pure SiO_2 nanotubes were successfully produced (ESI, Fig. S1 and S2a). Next, titania (TiO_2) was uniformly coated on the inner and outer surface of the SiO_2 nanotubes by means of co-precipitation (ESI, Fig. S1 and S2b). Then, TiO_2-coated SiO_2 nanotubes were chemically reduced via aluminothermic reduction reaction. Finally, we synthesized nanotubular Si-based multicomponents consisting of Si/Al_2O_3 and titanium silicide coating layers (Fig. 1b). The final product, titanium silicide-coated Si-based multicomponents, was firstly confirmed by X-ray diffraction (XRD) analysis (Fig. 1c). The XRD patterns showed the presence of Si (85.1 wt%), Al_2O_3 (9.5 wt%), and two types of titanium silicide ($Ti_5Si_3/TiSi_2$, 5.4 wt%) in the Si-based multicomponents.

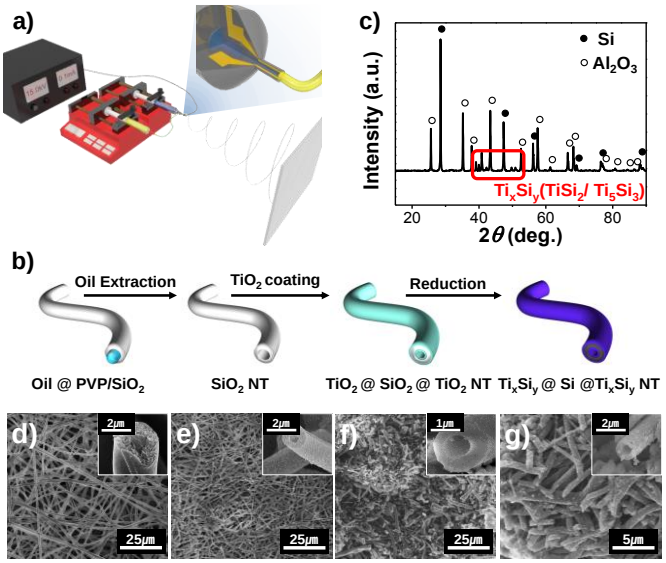

Fig. 1 (a) Schematic illustration of setup for coaxial electrospinning. The end-spinneret has separate paths for oil (inner) and polymer/inorganic solution (outer). (b) Experimental process for fabricating titanium silicide-coated Si-based multicomponent nanotubes. (c) XRD pattern of nanotubular Si-based multicomponents consisting of Si, Al_2O_3, and Ti_xSi_y. SEM images showing (d) SiO_2 precursor-containing PVP nanotubes, (e) pure SiO_2 nanotubes, (f) TiO_2-coated SiO_2 nanotubes, and (g) nanotubular Ti_xSi_y-coated Si-based multicomponent.

Figure 1d-1g show low-magnified and high-magnified (Inset) scanning electron microscopy (SEM) images of samples obtained from each process described in the schematic illustration (Fig. 1b). The detailed mechanism of the coaxial electrospinning process will be discussed later. With high stability, heavy mineral oil was stuck in the core part of tubes, which shows clear phase separation from the shell part containing PVP and silica source (Inset of Fig. 1d).

Pure SiO_2 nanotubes were produced with smooth surfaces and dense shells after oil extraction and calcination process in air (Fig. 1e). Then, the TiO_2 coating process was simply carried out by the co-precipitation method with the help of pre-coated polysaccharide (hydroxyl propyl cellulose, HPC). Firstly, numerous hydroxyl groups of HPC were strongly anchored to the surface of a SiO_2 nanotube. Secondly, a titanium precursor, titanium butoxide, was incorporated into the HPC covered sites in the SiO_2 nanotube and subsequent addition of deionized water led to the formation of TiO_2-coated SiO_2 nanotubes. When the obtained samples were thermally treated in air, the HPC polymer was completely removed while crystalline TiO_2-coated SiO_2 nanotubes were obtained (Fig. 1f and ESI, Fig. S1 and S2b). Crystalline phase of TiO_2 was matched with anatase after thermal annealing (ESI, Fig. S1). This will be converted to rutile phase during the metallothermic reduction. However, regardless of TiO_2 phase, complete conversion of crystalline TiO_2 to titanium silicide during the metallothermic reduction was observed. It should be noted that the TiO_2 layers were

Nanoscale Accepted Manuscript

distributed not only on the outer surface of the nanotubes, but also on the surface of the inner wall. As a final step, we employed metallothermic reduction which can be readily applied to a reduction of metal oxides. Based on the principles of the Ellingham diagram, various metal reductants (e.g., Mg, Al, Ca, etc.) are available.[61-65] Most metallothermic reductions are exothermic reactions which bring explosive thermal shock to the overall system. Accordingly, they have been suitable for manufacturing metal nanoparticles utilizing tremendous amounts of heat.[66, 67] In contrast, nanostructured metal oxides such as nanotubes, nanowires, and hollow spheres are easily damaged by thermal shock. When we carried out magnesiothermic reduction of SiO_2 nanotubes prepared in this study, all tubular structures totally collapsed due to the tremendous exothermic heat (ESI, Fig. S3). That is why we employed Al reductant which exhibits much lower exothermic heat compared to Mg.[68-70] At the same time, Al_2O_3 by-products formed by the aluminothermic reaction can act as a buffer layer for the structural integrity of Si-based anode materials (Equation 1). For these reasons, aluminothermic reduction of TiO_2-coated SiO_2 nanotubes is an effective strategy to make nanotubular Si-based materials. Another important point is that Al can reduce both SiO_2 and TiO_2 to Si and Ti, respectively, and titanium silicides can be formed at the interface between Ti (TiO_2) and Si. As described in the following equations, reduced Ti and Si can make titanium silicide with a form of $TiSi_2$ (Equation 2). Furthermore, from Equation 3 and Equation 4, titanium silicide with different composition also can be formed. The XRD pattern of Fig. 1c shows that two types of titanium silicide were successfully formed on the Si surface. It was coated on the inner and outer surface of Si nanotube walls as shown in the line scan profile and energy dispersive X-ray spectroscopy (EDS) mapping (Fig. 2f and 2g).

$$3SiO_2 + 4Al \rightarrow 3Si + 2Al_2O_3 \quad (1)$$

$$Ti + 2Si \rightarrow TiSi_2 \quad (2)$$

$$TiO_2 + 4Si \rightarrow TiSi_2 + 2SiO\uparrow \ (>900\ ^oC) \quad (3)$$

$$yTiSi_2 + (2x\text{-}y)Ti \rightarrow 2Ti_xSi_y \quad (4)\ [71\text{-}73]$$

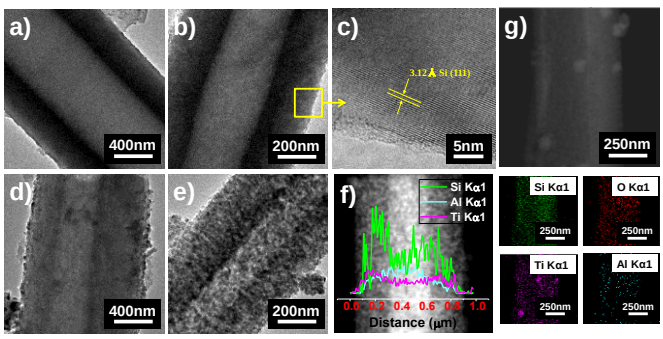

Fig. 2 TEM images of four types of nanotubes of (a) SiO_2, (b) Si, (c) Si taken from rectangular box seen in (b), (d) SiO_2@TiO_2, (e) Si@Ti_xSi_y, (f) line-scan graph of Si@Ti_xSi_y, and (g) EDS mapping images of Si@Ti_xSi_y.

After the aluminothermic reaction, a large amount of Al_2O_3 was contained in the nanotubular Si-based multicomponents. An excess amount of electrochemically inactive Al_2O_3 should be avoided. However, it is known that extremely stable Al_2O_3 phase (corundum) can be only etched by concentrated phosphoric acid or harsh mixture of acids at elevated temperature. In case of phosphoric acid, it can eliminate metal silicides as well as Al_2O_3. Thus, proper etching condition should be used to preserve the tubular structure and to selectively remove Al_2O_3. If we etched Al_2O_3 completely from the Si-based multicomponents (e.g., at 150 ^oC for more than 2 h), tubular structure was fatally damaged, leading to eventual collapse to form almost nanoparticle (ESI, Fig. S4a-4d). Their electrochemical performance showed a fast capacity decaying results, due to a lack of structural integrity, while TixSiy-coated Si nanotube (without Al_2O_3 layer) exhibited significantly improved cycling performance (ESI, Fig. S4e and S4f). Through an optimized leaching process (at 150 ^oC for 90 min) in concentrated phosphoric acid, 4-5 wt% of Al_2O_3 was left over in the Si-based materials to increase structural integrity of the final multicomponent anodes during battery operation. Finally, nanotubular structured Ti_xSi_y-coated Si/Al_2O_3 multicomponents were successfully synthesized as shown in Fig. 1c and Fig. 2e-2g. Additionally, we also prepared Si-based nanotubes without titanium silicide coating layers. Even in the absence of TiO_2 coating layers, SiO_2 nanotubes (Fig. 2a) were successfully converted to Si nanotubes via the aluminothermic reduction process without a significant morphology change (Fig. 2b and ESI, Fig. S5). A high-magnified TEM image of as-synthesized Si nanotubes shows lattice fringes of 0.312 nm that are consistent with the typical d-spacing value of Si (111) plane (Fig. 2c).

Initially, bare Si/Al_2O_3 nanotubes were simply fabricated via aluminothermic reduction of SiO_2 nanotubes. Fig. 2a shows a TEM image of pristine SiO_2 nanotubes which have a highly smooth surface with nanotubular structure. After chemical reduction of the SiO_2 nanotubes, as-synthesized Si/Al_2O_3 nanotubes kept the original nanotubular shape, but made the diameter smaller due to removal of oxygen during the aluminothermic reduction (Fig. 2b). When TiO_2 layers were coated on the surface of the inner and outer walls of SiO_2 nanotubes, nanotubular TiO_2-coated SiO_2 (SiO_2@TiO_2) was successfully obtained without destroying the original morphology of the SiO_2 nanotubes (Fig. 2d). Subsequent aluminothermic reduction of the SiO_2@TiO_2 sample led to the formation of tubular shaped Ti_xSi_y-coated porous Si/Al_2O_3 (Si@Ti_xSi_y) (Fig. 2e). As shown in line scan profiles of Fig. 2f and EDS mapping of Fig. 2g, Al_2O_3, by-products formed by aluminothermic reduction and Ti (in the form of Ti_xSi_y) were uniformly distributed over the entire tubular structure. In addition, we prepared also carbon-coated Si nanotubes simply by thermal deposition of toluene at 900 ^oC for 8 min that is optimized conditions. Amount of carbon coating layers was characterized by the elemental analysis (~9 wt%) and Raman spectroscopy. Raman spectrum of carbon-coated Si nanotubes exhibited the ratio of disordered (D) band and graphene (G) band (D/G ratio) is 2.08, demonstrating that amorphous carbon layers were coated on the surface of Si-based nanotubes (ESI, Fig. S6).

Tuning of dimension of SiO_2 nanotubes

Nanoscale Accepted Manuscript

This journal is © The Royal Society of Chemistry 2014

The dimension of SiO_2 nanotubes is easily tunable by controlling the coaxial electrospinning process. The coaxial electrospinning process is composed of two steps: (i) stabilization between two different liquids and (ii) pulling out continuous stretching fibers under an electric field. The first step is the crucial part to determine whether or not the whole electrospinning process could work. Two different solutions are joined together at the end of a dual nozzle. If they cannot form a stable interface, they get mixed up so that no tubular shape fibers will be obtained. In our case, the solvent for the polymer solution is ethanol, which can disentangle the heavy oil into itself. Regulating this instability can be done by tuning the pumping rate of both oil and polymer solution. In particular, this system was strongly dependent on oil rate. If the oil rate exceeds a certain level, clear separation of core and sheath cannot be formed. To form continuous hollow fibers, the feeding rate of oil requires at least 0.5 μL min^{-1}. Below this rate (e.g., 0.01 μL min^{-1}), no pore was formed (ESI, Fig. S7a). Conversely, when coaxial spinning was carried out at the upper limit of the feeding rate (10 μL min^{-1}), spinnability dramatically decreased, indicating that 1D structure was hardly observed and most of the fibers were merged together (ESI, Fig. S7c and 7d). Through an optimization process, we could get the appropriate feeding rate of 0.5-5 μL min^{-1}. All of the following experiments were carried out with a feeding rate of 1 μL min^{-1} at applied bias of 23 kV. Initially, we applied 10 kV of voltage at early stage of electrospinning. But, in low voltage range from 10 kV to 20 kV, the polymeric fibers cannot be formed continuously. At these voltage ranges, electrospinning jet was converted to spray-like jet. Above 20 kV, we can obtain continuous polymeric fibers, which did not show any dependency on applied voltage over the lower limit of 20 kV to 25 kV (maximum load for potentiostat).

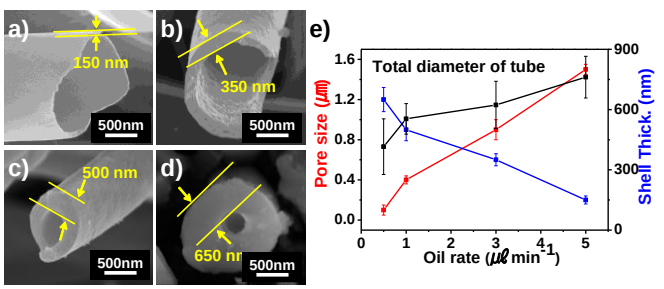

Fig. 3 SEM images of SiO_2 tubes fabricated from different feeding rates of heavy oil at a fixed feeding rate (0.9 mL h^{-1}) of polymer solution. The oil feeding rates are (a) 5, (b) 3, (c) 1, and (d) 0.5 μL min^{-1}, respectively. (e) Plots of pore size and shell thickness variation as a function of oil feeding rate.

Also, the voltage close to maximum load was avoided for safety issue. That is why we selected 23 kV of voltage as optimum load. The second step is how well the polymer sheath solution undergoes a strong electric field forming continuous fibers. Under applied voltage ranges of 20-25 kV, charged molecules are subject to rapid stretching between capillary and collector. This can cause powerful viscous force tangential to the feeding direction. Accordingly, the sheath solution has force to pull the core out so that oil can be located in the core position with high stability.

When we varied the feeding rate of heavy oil from 0.5 to 5 μL min^{-1} at a fixed feeding rate (0.9 mL h^{-1}) of polymer solution, it was shown that the total diameter of tubes did not change significantly. As the oil feeding rate was increased, total diameter of tubes is slightly increased. This is because faster feeding rate engages instability on overall tubular formation. As a result, dimension of tubes are increased for holding internal pressure. The higher the oil feeding rate was used, the larger pores and the thinner shells are formed (Fig. 3). We added error bars based on the results obtained from reproducibility test. In addition, it is also important to extract the heavy mineral oil from the core part, because remaining oil can act as impurities during the metallothermic reaction. In fact, the length scale of fibers obtained by electrospinning could be approximately hundreds of micrometer to a few millimeter. After soaking as-spun fibers in n-hexane for 1 day, when we observed the middle part of broken long fibers, complete holes were not made, indicating the existence of residual oil (ESI, Fig. S7b). That is why intensive heat treatment was required to completely remove all the residual oils and polymers at 600 °C for 3h at air. Eventually, at a fixed feeding rate of 0.9 mL h^{-1} of sheath solution, we concluded that oil feeding rate of 1 μL min^{-1} under applied voltage of 23 kV (at 10 cm tip to collector distance), were optimum condition for electrospinning. All the following electrochemical tests were conducted with Si-based nanotubes fabricated by optimum conditions.

Electrochemical performances of nanotubular Si-based anodes

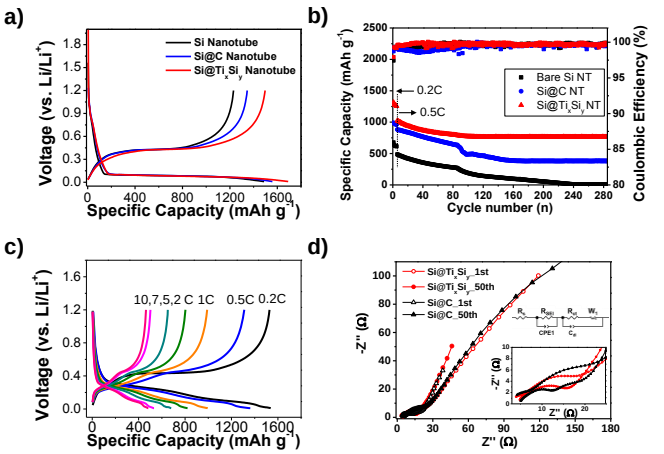

Figure. 4 (a) Galvanostatic charge/discharge profiles of different Si-based nanotubes at 0.05C. (b) Cycling performances and coulombic efficiency of nanotube electrodes at 0.2 C (1^{st}-5^{th} cycles) and at 0.5 C (6^{th}-285^{th} cycles). (c) Rate capability of Ti_xSi_y-coated Si nanotube electrode (discharge/charge rates are the same). (d) Electrochemical impedance spectra of carbon-coated and Ti_xSi_y-coated Si nanotubes after 1^{st} and 50^{th} cycles.

Up to now, the surfaces of Si-based anodes and cathode materials with poor electrical conductivity have been modified to improve their electrochemical performance. In general, the surface coating process requires cumbersome steps and thermal treatment at elevated

Nanoscale Accepted Manuscript

temperature which might cause a negative effect on active materials. In contrast, titanium silicide coating can be easily achieved during the synthetic process of Si-based anode materials, in which the conversion of SiO_2 to Si and titanium silicide coating proceeds simultaneously without an additional heat treatment step. In addition to the simple process, titanium silicide coating layers with high mechanical and electrical conductivity would increase the electrochemical properties of Si-based electrodes

We investigated the electrochemical properties of Si nanotubes, carbon-coated Si nanotubes, and Ti_xSi_y-coated Si nanotube electrodes in a coin-type half-cell (2016R type). The first cycle galvanostatic voltage profiles are shown in Fig. 4a in the cut-off voltage range of 0.01-1.2 V at a rate of 0.05 C. The first discharge (lithiation) and charge (delithiation) capacity of bare Si nanotubes without any coating layers are 1,488 mAh g^{-1} and 1,230 mAh g^{-1}, respectively, corresponding to a coulombic efficiency of 82.6% (Fig. 4a**)**. Carbon-coated Si nanotubes shows a first discharge capacity of 1570 mAh g^{-1} with a higher coulombic efficiency of 86.3%. This enhancement is attributed to a decrease of surface resistance at an early stage of discharge. And, Ti_xSi_y-coated Si nanotubes exhibit a first discharge capacity of 1741 mAh g^{-1} with the highest coulombic efficiency of 88.5%. This extraordinary improvement results from characteristics of Ti_xSi_y layers which provide high electrical conductivity and form a stable solid-electrolyte-interface (SEI) layer.[52] Considered the cycling stability of Si-based anode materials, electrical conductivity, stable SEI formation, and mechanical strength during cycling should be appropriately combined together. From this point of view, Ti_xSi_y-coated Si nanotubes have both advantages and exhibit superior cycling stability (capacity retention of ~75% after 280 cycles at the same discharge/charge of 0.5 C rate) (Fig. 4b). In contrast, bare Si nanotubes and carbon-coated Si nanotubes show capacity retention of only 2% and 43% after 280 cycles, respectively (Fig. 4b).

Without any protective layers on Si nanotube surface, tubular-type will be easily collapsed. It demonstrated that only structural effect was not enough to redeem the disadvantages of Si, such as a large volume expansion, low lithium ion conductivity, and continuous SEI formation derived from active material exposure. In contrast, when thin carbon layers were coated on the surface of Si nanotubes, it showed better cycling stability by enhancing electrical conductivity of Si and acting as a protective layer for a serious side reaction between electrolyte and active material. Nonetheless, the carbon-coated Si nanotubes continuously reacted with electrolyte, leading to the formation of a continuous SEI layer. After 150 cycles, it was stabilized at charge capacity of ~380 mAh g^{-1}. On the other hand, Ti_xSi_y-coated Si nanotubes showed outstanding electrochemical properties in long-term cycling test. The excellent electrochemical properties of Ti_xSi_y-coated Si nanotubes can be explained as follows: (i) good mechanical properties of Ti_xSi_y and Al_2O_3 maintain structural integrity of Si nanotubes, (ii) both Ti_xSi_y and Al_2O_3 coating layers induce the formation of highly stable SEI layers on the Si surface,[50,52] and (iii) nanotubular Si structure and mesopores formed by reduction of SiO_2 significantly improve accessibility of lithium ions and liquid electrolytes. Moreover, when tubular-type Si electrodes were cycled at different C-rate ranging from 0.2 C to 10 C (with the same discharge/charge rate), it is noteworthy that the Ti_xSi_y-coated Si nanotubes showed an excellent rate capability (483 mAh g^{-1}, specific capacity of 36.9 % even at 10 C, compared to 0.5 C rate) as shown in Fig. 4c. In contrast, bare and carbon-coated Si nanotubes showed poor rate capabilities of 4.5% and 8.3% in the same experimental condition, respectively (EIS, Fig. S8a and 8b). The Ti_xSi_y-coated Si nanotubes exhibited the electrochemical properties in both rate capability and cycle retention.

Along with the optimized tubes, we also investigated the electrochemical performances of Si-based nanotubes with thin (100-200 nm) and thick (600-700 nm) shell layers. Thin tubes showed almost similar cycling stability to the optimized case, while thick tubes exhibited relatively fast capacity fading (EIS, Fig. S9). As the shell size get thicker, its tubular structure is collapsed to form seriously aggregated structure without any tubes or pores during the metallothermic reduction process. This result leads to the retardation of lithium ion transport and finally a fast capacity loss. In addition, Ti_xSi_y-coated Si nanotubes without Al_2O_3 shows higher discharge capacity (1860 mAh g^{-1}), but low charge capacity (1497 mAh g^{-1}), which corresponds to a coulombic efficiency of 80.5%. Slightly increased discharge capacity is attributed to removal of electrochemically inactive Al_2O_3 layer. However, good mechanical property of Al_2O_3 cannot be used for structural integrity during the cycling process. The resulting Si nanotube electrode showed worse cycling property than Si nanotubes with Al_2O_3 layer (ESI, Fig. S4e and 4f).

Characterization of nanotubular Si-based anodes

In order to gain better understanding of the enhanced cycling stability and rate capability of Ti_xSi_y-coated Si nanotubes compared to bare Si nanotubes and carbon coated Si nanotubes, electrochemical impedance spectroscopy (EIS) measurements were carried out at different cycling points (1^{st} and 50^{th} cycles). Fig. 4d presents a typical curve of Nyquist plot ranging from 100 KHz to 0.1 Hz with an amplitude of 10 mV. Also we added an equivalent circuit model (inset of Fig. 4d). R_s represents the electrolyte resistance which corresponds to the intercept of the semicircle in a higher frequency range, while R_{SEI} represents SEI layer resistance. R_{ct} and C_{dl} are the charge transfer resistance and related double layer capacitor in the middle frequency region, respectively. As shown in spectra, filled symbol shows a clear difference in semicircle size. Smaller sized semicircle at high frequencies was observed for Ti_xSi_y-coated Si nanotube electrodes after 1^{st} and 50^{th}, indicating lower charge transfer resistance. At 1^{st} cycle, the Ti_xSi_y-coated Si nanotubes only showed one semicircle at high frequency region, while carbon-coated Si nanotubes had double circles, which are attributed to a thick and uniform carbon coating layer on Si nanotubes. After 50^{th} cycling, both electrodes exhibited a big semicircle (evidence for a formation of SEI layer) in high-middle frequency region. From the fitting for resistance of SEI formation, Ti_xSi_y coated Si nanotubes showed much lower values, implying that much more uniform and thinner SEI layers are formed on top of the electrode surface. Also, charge transfer resistance of the Ti_xSi_y-coated Si nanotubes (10.53 Ω) is significantly reduced compared to the carbon-coated electrode (29.26 Ω), demonstrating the effect of electrically and mechanically beneficial Ti_xSi_y layers on the electrochemical properties of Si-based multicomponents.

Nanoscale Accepted Manuscript

 This journal is © The Royal Society of Chemistry 2014

In addition, to use them as practical LIB anodes, it is critical to investigate how much the electrodes experience volume expansion. Fig. 5 displays cross-sectional SEM images of three types of Si nanotube electrodes before cycles and after 100 cycles at a 0.5 C rate. The theoretical volume expansion of Si is >300% when Si takes 3.5 lithium ions at room temperature. In conventional Si nanoparticles or other Si-based nanostructures, it cannot bear a large volume expansion occurring during fully lithiation process, resulting in crack on the surface of Si materials or deformation of the original Si structure. Thus, even delicately fabricated Si nanostructures cannot recover their original shapes. Accordingly, direct exposure of Si materials to electrolytes through the cracks produces continuous SEI formation on the surface of Si particles. In this perspective, titanium silicide on the Si nanotubes can promote surface stabilization, which, in turn, induces stable, uniform, and conformal SEI formation on the surface of Si nanotubes. As a result, SEI formed at early stage of cycles is well-sustained during the repeated cycles. In addition, structural integrity of nanotubular structured Si by titanium silicide and alumina can suppress real expansion of Si nanotubes. These are indirectly demonstrated through SEM (thickness change of electrode) and TEM (volume expansion of Si-based materials) analyses. Firstly, three electrodes showed greatly suppressed volume expansion, which is attributed to porous structure and existed void space in electrodes. Even bare Si nanotubes exhibited volume expansion of 55.5% after 100 cycles (Fig. 5a), while the carbon-coated Si nanotube electrode showed a reduced volume expansion of 30% (Fig. 5b). Surprisingly, Ti_xSi_y-coated Si nanotubes exhibited a volume expansion of only 15% (Fig. 5d), suggesting that the tubular structure and surface stabilization by titanium silicide contribute to a remarkable suppression of volume expansion.

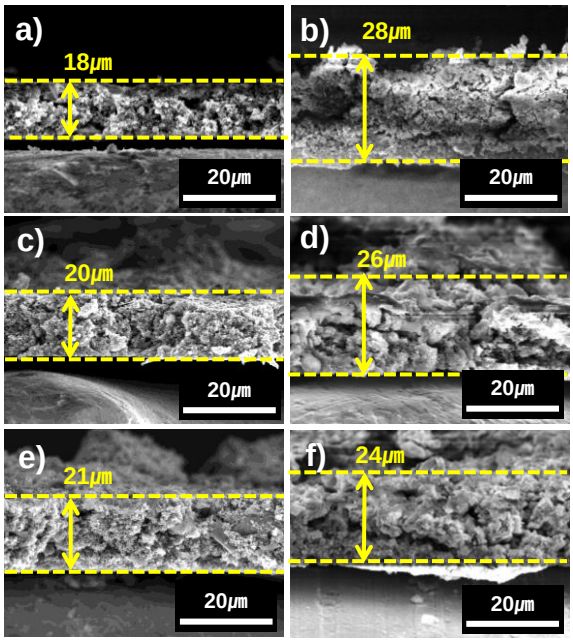

Fig. 5 Cross-sectional SEM images of electrodes fabricated from three types of Si nanotubes: (a-b) bare Si, (c-d) carbon coated Si, and (e-f) Ti_xSi_y-coated Si before cycling (a, c, e) and after 100 cycles (b, d, f).

In addition, we conducted TEM analysis on microscopic structural change of multicomponent Si nanotube anodes after 100 cycles at 0.5 C rate (EIS, Fig. S10). Without any help of surface coating layers, bare Si nanotubes cannot endure the large volume expansion during the repeated cycles. Tubular structure was almost collapsed and its surface was covered with thick SEI layers from direct exposure of Si surface to electrolyte (EIS, Fig. S10a-c). Thus, tubes cannot be recovered to original structure. In case of carbon coated one, tubular structure was well maintained. However, shell thickness of tubes was increased to 700-800 nm (corresponding to total diameter of 2.2 μm) compared to initial thickness of 500-600 nm (total diameter of 1.6 μm), corresponding to a volume expansion of 38-40% (EIS, Fig. S10d and S10e). Uniformed coated carbon layers on the Si tubes cannot be helpful for recovering the structure and formation of stable SEI. High magnification TEM image of this outer shell shows the existence of thick SEI layers (EIS, Fig. S10f). Interestingly, Ti_xSi_y-coated Si nanotubes evenly expanded to radial direction with a volume expansion of ~15%, corresponding to diameter of 550-650 nm (Fig. S10g and 10h). Any types of crack or bursting tubes were not observed. This outmost shell was quite smooth and covered with 10 nm thick uniform SEI layers (EIS, Fig. S10i). These results are consistent with change of electrode thickness as shown in Fig. 5. Ti_xSi_y and Al_2O_3 layers provided excellent structural integrity and interfacial stability to the Si-based anodes. As a result, we may solve a chronic problem: the low volumetric energy density which arises from highly expanded Si during cycling of Si-based anode materials and continuous capacity fading from side reactions of Si with electrolyte. Most Si-based anodes (except for nanostructured materials such as nanoparticles, nanowires, and nanotubes) exhibit dramatic capacity fading (<50% of initial capacity) during early stage of cycles, which is originated from structural collapse during lithiation and failure in structure recovery (ESI, Table S1). However, our Si-based multicomponents show structural stability and also greatly stable rate capability at the same high charge-discharge rate. In particular, even though other Si nanotubes or Si nanowires show high capacity at early stage, our Si-based multicomponents deliver much stable cycling retention and rate capability considering current density and loading mass.

Conclusion

We have successfully integrated the coaxial electrospinning method and aluminothermic reduction process for the first time. Coaxial electrospinning enabled us to produce nanotubular structured silica materials with tunable thickness and diameter, while aluminothermic reaction led to the formation of Si-based multicomponents consisting of Si and Al_2O_3. In particular, when titania coating layers were introduced to silica nanotubes, titanium silicides with good mechanical and high electrical properties were simultaneously formed on the Si-based multicomponents during the aluminothermic reaction. When electrochemical performances of the resulting anodes were evaluated, superior results are obtained. Synergistic coupling of tubular structure, structural integrity, and interfacial stability from titanium silicide and alumina resulted in remarkably enhanced

Nanoscale Accepted Manuscript

electrochemical properties of Si-based multicomponent electrodes including a stable cycling property (765 mAh g^{-1} after 280 cycles at 0.5C), superior high rate capability (483 mAh g^{-1} at 10C/10C), and significantly reduced volume change (electrode expansion of 14%). Furthermore, it was demonstrated that stable, thinner, and uniform SEI layers were formed on the Si electrode surface to suppress structural collapse, comparing with other types of tubes from the TEM analysis of cycled electrodes. This synthetic strategy can be extended to other anode and cathode materials which require electrical conductivity, easy access of electrolyte and lithium ions, and structural integrity.

Acknowledgements

This work was supported by the IT R&D program of MOTIE/KEIT (10046309).

Notes and references

Department of Energy Engineering, School of Energy and Chemical Engineering, Ulsan National Institute of Science and Technology (UNIST), UNIST-gil 50, Ulsan 689-798, Republic of Korea. Fax: +82-52-217-2909; Tel: +82-52-217-2515
E-mail: spark@unist.ac.kr

† Electronic Supplementary Information (ESI) available. See DOI: 10.1039/c000000x/

1. J. R. Szczech and S. Jin, *Energy Environ. Sci.*, 2011, **4**, 56-72.
2. X. L. Li and L. J. Zhi, *Nanoscale*, 2013, **5**, 8864-8873.
3. M. T. McDowell, S. W. Lee, J. T. Harris, B. A. Korgel, C. M. Wang, W. D. Nix and Y. Cui, *Nano Lett.*, 2013, **13**, 758-764.
4. A. S. Arico, P. Bruce, B. Scrosati, J. M. Tarascon and W. Van Schalkwijk, *Nat. Mater.*, 2005, **4**, 366-377.
5. P. G. Bruce, B. Scrosati and J. M. Tarascon, *Angew. Chem., Int. Ed.*, 2008, **47**, 2930-2946.
6. T. L. Kulova, A. M. Skundin, Y. V. Pleskov, E. I. Terukov and O. I. Kon'kov, *J. Electroanal. Chem.*, 2007, **600**, 217-225.
7. J. C. Li, X. C. Xiao, F. Q. Yang, M. W. Verbrugge and Y. T. Cheng, *J. Phys. Chem. C*, 2012, **116**, 1472-1478.
8. R. Mukherjee, R. Krishnan, T. M. Lu and N. Koratkar, *Nano Energy*, 2012, **1**, 518-533.
9. E. Pollak, G. Salitra, V. Baranchugov and D. Aurbach, *J. Phys. Chem. C*, 2007, **111**, 11437-11444.
10. J. Xie, N. Imanishi, T. Zhang, A. Hirano, Y. Takeda and O. Yamamoto, *Mater. Chem. Phys.*, 2010, **120**, 421-425.
11. Y. M. Lin, K. C. Klavetter, P. R. Abel, N. C. Davy, J. L. Snider, A. Heller and C. B. Mullins, *Chem. Commun.*, 2012, **48**, 7268-7270.
12. X. S. Zhou and Y. G. Guo, *J. Mater. Chem. A*, 2013, **1**, 9019-9023.
13. J. P. Maranchi, A. F. Hepp and P. N. Kumta, *Electrochem. Solid State Lett.*, 2003, **6**, A198-A201.
14. S. K. Soni, B. W. Sheldon, X. C. Xiao, M. W. Verbrugge, D. Ahn, H. Haftbaradaran and H. J. Gao, *J. Electrochem. Soc.*, 2012, **159**, A38-A43.
15. X. Xiao, P. Liu, M. W. Verbrugge, H. Haftbaradaran and H. Gao, *J. Power Sources*, 2011, **196**, 1409-1416.
16. C. J. Yu, X. Li, T. Ma, J. P. Rong, R. J. Zhang, J. Shaffer, Y. H. An, Q. Liu, B. Q. Wei and H. Q. Jiang, *Adv. Energy. Mater.*, 2012, **2**, 68-73.
17. B. M. Bang, H. Kim, J. P. Lee, J. Cho and S. Park, *Energy Environ. Sci.*, 2011, **4**, 3395-3399.
18. C. K. Chan, H. L. Peng, G. Liu, K. McIlwrath, X. F. Zhang, R. A. Huggins and Y. Cui, *Nat. Nanotechnol.*, 2008, **3**, 31-35.
19. B. Hertzberg, A. Alexeev and G. Yushin, *J. Am. Chem. Soc.*, 2010, **132**, 8548-8549.
20. H. Ma, F. Y. Cheng, J. Chen, J. Z. Zhao, C. S. Li, Z. L. Tao and J. Liang, *Adv. Mater.*, 2007, **19**, 4067-4070.
21. M. H. Park, M. G. Kim, J. Joo, K. Kim, J. Kim, S. Ahn, Y. Cui and J. Cho, *Nano Lett.*, 2009, **9**, 3844-3847.
22. T. Song, J. L. Xia, J. H. Lee, D. H. Lee, M. S. Kwon, J. M. Choi, J. Wu, S. K. Doo, H. Chang, W. Il Park, D. S. Zang, H. Kim, Y. G. Huang, K. C. Hwang, J. A. Rogers and U. Paik, *Nano Lett.*, 2010, **10**, 1710-1716.
23. H. Wu, G. Chan, J. W. Choi, I. Ryu, Y. Yao, M. T. McDowell, S. W. Lee, A. Jackson, Y. Yang, L. B. Hu and Y. Cui, *Nat. Nanotechnol.*, 2012, **7**, 309-314.
24. H. Wu, G. Y. Zheng, N. A. Liu, T. J. Carney, Y. Yang and Y. Cui, *Nano Lett.*, 2012, **12**, 904-909.
25. Y. Yao, M. T. McDowell, I. Ryu, H. Wu, N. A. Liu, L. B. Hu, W. D. Nix and Y. Cui, *Nano Lett.*, 2011, **11**, 2949-2954.
26. K. J. Zhao, M. Pharr, L. Hartle, J. J. Vlassak, Z. G. Suo, *J. Power Sources*, 2012, **218**, 6-14.
27. W. K. Choi, T. H. Liew, M. K. Dawood, H. I. Smith, C. V. Thompson and M. H. Hong, *Nano Lett.*, 2008, **8**, 3799-3802.
28. J. de Boor, N. Geyer, J. V. Wittemann, U. Gosele and V. Schmidt, *Nanotechnology*, 2010, **21**.
29. A. I. Hochbaum, R. Fan, R. R. He and P. D. Yang, *Nano Lett.*, 2005, **5**, 457-460.
30. N. M. Hwang, W. S. Cheong, D. Y. Yoon and D. Y. Kim, *J. Cryst. Growth*, 2000, **218**, 33-39.
31. S. Sharma, T. I. Kamins and R. S. Williams, *Appl. Phys. A: Mater. Sci. Process.*, 2005, **80**, 1225-1229.
32. T. H. Hwang, Y. M. Lee, B. S. Kong, J. S. Seo and J. W. Choi, *Nano Lett.*, 2012, **12**, 802-807.
33. L. W. Ji and X. W. Zhang, *Carbon*, 2009, **47**, 3219-3226.
34. X. S. Zhou, L. J. Wan and Y. G. Guo, *Small*, 2013, **9**, 2684-2688.
35. J. K. Yoo, J. Kim, Y. S. Jung and K. Kang, *Adv. Mater.*, 2012, **24**, 5452-5456.
36. J. Zhu, H. L. Peng, S. T. Connor and Y. Cui, *Small*, 2009, **5**, 437-439.
37. X. Chen, A. Berger, M. Y. Ge, S. Hopfe, N. Dai, U. Gosele, S. Schlecht and M. Steinhart, *Chem. Mater.*, 2011, **23**, 3129-3131.
38. Y. J. Chen, X. Y. Xue and T. H. Wang, *Nanotechnology*, 2005, **16**, 1978-1982.
39. N. I. Kovtyukhova, T. E. Mallouk and T. S. Mayer, *Adv. Mater.*, 2003, **15**, 780-785.
40. H. Ogihara, S. Takenaka, I. Yamanaka, E. Tanabe, A. Genseki and K. Otsuka, *Chem. Mater.*, 2006, **18**, 996-1000.
41. C. H. Ruscher, I. Bannat, A. Feldhoff, L. R. Ren and M. Wark, *Microporous Mesoporous Mater.*, 2007, **99**, 30-36.
42. C. -L. Zhang and S. -H. Yu, *Chem. Soc Rev.*, 2014, 43, 4423-4448
43. H. Han, T. Song, J.Y. Bae, L.F. Nazar, H. Kim and U. Paik, *Energy Environ. Sci.*, 2011, **4**, 4532-4536.
44. Z. Kurban, A. Lovell, S.M. Bennington, D.W.K. Jenkins, K.R. Ryan, M.O. Jones, N.T. Skipper and W.I.F. David, *J. Phys. Chem. C*, 2010, **114**, 21201-21213.
45. D. Li and Y. N. Xia, *Nano Lett.*, 2004, **4**, 933-938.
46. D. G. Yu, C. Branford-White, K. White, N. P. Chatterton, L. M. Zhu, L. Y. Huang and B. Wang, *Express Polym. Lett.*, 2011, **5**, 732-741.
47. T. Yuan, B. T. Zhao, R. Cai, Y. K. Zhou and Z. P. Shao, *J. Mater. Chem.*, 2011, **21**, 15041-15048.
48. N. E. Zander, *Polymers*, 2013, **5**, 19-44.
49. R. Huang, X. Fan, W. C. Shen and J. Zhu, *Appl. Phys. Lett.*, 2009, **95**.
50. J. C. Guo, A. Sun, X. L. Chen, C. S. Wang and A. Manivannan, *Electrochim. Acta*, 2011, **56**, 3981-3987.
51. N. Dimov, K. Fukuda, T. Umeno, S. Kugino and M. Yoshio, *J. Power Sources*, 2003, **114**, 88-95.
52. J. K. Lee, W. Y. Yoon and B. K. Kim, *J. Electrochem. Soc.*, 2013, **160**, A1348-A1352.
53. M. Yoshio, H. Y. Wang, K. Fukuda, T. Umeno, N. Dimov and Z. Ogumi, *J. Electrochem. Soc.*, 2002, **149**, A1598-A1603.
54. P. F. Gao, J. W. Fu, J. Yang, R. G. Lv, J.L. Wang, Y. N. Nuli and X. Z. Tang, *Phys. Chem. Chem. Phys.*, 2009, **11**, 11101-11105.
55. S. Murugesan, J. T. Harris, B. A. Korgel and K. J. Stevenson, *Chem. Mater.*, 2012, **24**, 1306-1315.
56. Y. He, X. Yu, Y. Wang, H. Li and X. Huang, *Adv. Mater.*, 2011, 23, 4938-494.

Nanoscale Accepted Manuscript

 This journal is © The Royal Society of Chemistry 2014

57. H. Park, S. Lee, S. Yoo, M. Shin, J. Kim, M. Chun, N.S. Choi and S. Park, *ACS Appl. Mater. Inter.*, 2014, **6**, 16360-16367.
58. O. Park, J. I. Lee, M. J. Chun, J. T. Yeon, S. Yoo, S. Choi, N.S. Choi and S. Park, *RSC Adv.*, 2013, **3**, 2538-2542.
59. E. M. Lotfabad, P. Kalisvaart, A. Kohandehghan, K. Cui, M. Kupsta, B. Farbod and D. Mitlin, *J. Mater. Chem. A*, 2014, **2**, 2504-2516.
60. H. C. M. Knoops, M. E. Donders, M. C. M. van de Sanden, P. H. L. Notten and W. M. M. Kessels, *J. Vac. Sci. Technol. A*, 2012, **30**.
61. A. D. Mazzoni and E. F. Aglietti, *Appl. Clay Sci.*, 2000, **17**, 127-140.
62. A. Xing, J. Zhang, Z.H. Bao, Y. F. Mei, A. S. Gordin and K. H. Sandhage, *Chem. Commun.*, 2013, **49**, 6743-6745.
63. R. A. Sharma and R. N. Seefurth, *J. Electrochem. Soc.*, 1988, **135**, 66-71
64. R. O. Suzuki, *J. Phys. Chem. Solids*, 2005, **66**, 461-465.
65. Z. H. Bao, M. R. Weatherspoon, S. Shian, Y. Cai, P. D. Graham, S. M. Allan, G. Ahmad, M. B. Dickerson, B. C. Church, Z. T. Kang, H. W. Abernathy, C. J. Summers, M. L. Liu and K. H. Sandhage, *Nature*, 2007, **446**, 172-175.
66. C. W. Won, H. H. Nersisyan, H. I. Won and J. H. Lee, *Curr. Opin. Solid State Mater. Sci.*, 2010, **14**, 53-68.
67. Z. Favors, W. Wang, H. H. Bay, Z. Mutlu, K. Ahmed, C. Liu, M. Ozkan and C. S. Ozkan, *Sci. Rep.*, 2014, **4**.
68. K. Yasuda and T. H. Okabe, *J. Jpn. Inst. Met.*, 2010, **74**, 1-9.
69. R. A. Andrievskii, S. E. Kravchenko and S. P. Shilkin, *Inorg. Mater.*, 1995, **31**, 965-968.
70. R. A. Cutler, K. M. Rigtrup and A. V. Virkar, *J. Am. Ceram. Soc.*, 1992, **75**, 36-43.
71. F. Z. Zhao, X. F. Cui, B. Wang and J. G. Hou, *Appl. Surf. Sci.*, 2006, **253**, 2785-2791.
72. M. Berti, A. V. Drigo, C. Cohen, J. Siejka, G. G. Bentini, R. Nipoti and S. Guerri, *J. Appl. Phys.*, 1984, **55**, 3558-3565.
73. J. Trambukis and Z. A. Munir, *J. Am. Ceram. Soc.*, 1990, **73**, 1240-1245.

Nanoscale Accepted Manuscript